Effect of Surface Roughness on Deflagration-to-Detonation Transition in Submilimeter Channels

Ryan W. Houim and Elaine Oran
University of Maryland
College Park, Maryland, USA

1 Introduction

Reactive fuel-oxygen mixtures can be prone to detonation [1], which can present significant safety hazards or can be use to enhance thrust in propulsion applications [2–4]. Fundamental mechanisms of deflagration-to-detonation transition (DDT) are not well understood, despite its long history of research.

Though DDT in experiments usually occurs in the presence of turbulent flames in obstacle-laden channels, acceleration of laminar flames can also lead to detonation. One example is flame propagation in submillimeter channels and gaps [4–10]. In these thin channels a precursor shock is produced as the flame accelerates, which creates a boundary layer in front of the flame. A combination of shock heating and viscous dissipation can increase the temperature in the boundary layer until autoignition occurs [5, 11, 12]. The resulting spontaneous wave, in turn, leads to the initiation of a detonation.

The large distance and time required for a detonation to initiate in a smooth channel limits the practicality and pulsing frequency of detonation-based microthrusters [3, 4]. Typically, obstructions, such as Shchelkin spirals [13] are used to promote DDT in detonation-based combustors. It is not practical, however, to place similar obstacles in submillimeter channels. Instead, microfabrication techniques have been used to etch microscale features into submilimeter channels [4]. The height of these microscale features are too small to be treated as traditional obstacles and, as a result, they can be considered as large surface roughness elements.

Detailed understanding on the influence of surface roughness on DDT has not been extensively studied. To help understand how surface roughness influences DDT in submillimeter tubes, this paper presents three-dimensional numerical simulations of DDT in channels with varying degrees of wall roughness.

2 Physical Model and Geometrical Setup

The numerical model solves the unsteady, compressible, reactive Navier-Stokes equations. The reactants are a stoichiometric mixture of C_2H_4 and oxygen. A simplified chemical-diffusive model with single-step

Correspondence to: rhouim@umd.edu

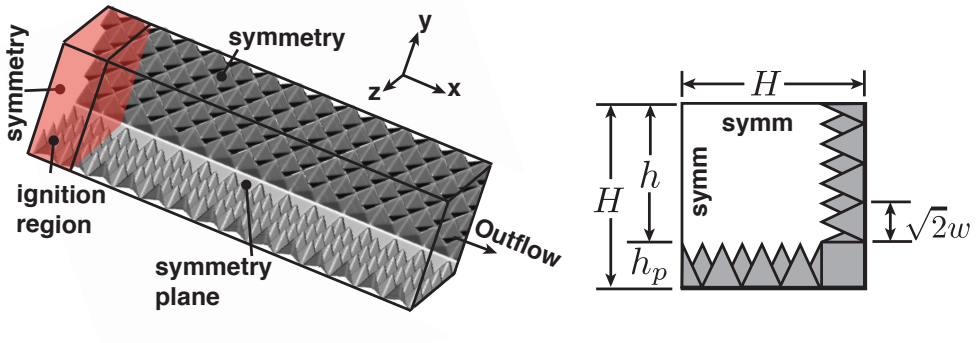

Figure 1: Three-dimensional and cross-sectional views of the geometrical setup.

irreversible chemistry and constant specific heat is used [5]. The chemical reaction is given by

$$\mathrm{R} + \mathrm{M} \rightarrow \mathrm{P} + \mathrm{M}, \tag{1}$$

where R, P, and M, are the reactants, products, and a third body. The chaperon efficiency of reactants and products is taken to be unity. The prefactor and activation temperature are 3.255×10^{10} m^3/kmol-s and 11,682 K, respectively. The chemical energy release from this reaction is 4.77 MJ/kg of reactant. The mass diffusivity is computed using

$$\mathcal{D} = \mathcal{D}_0 \frac{T^{0.7}}{\rho}, \tag{2}$$

where $\mathcal{D}_0 = 1.0 \times 10^{-6}$ kg/s-m-K$^{0.7}$ and ρ and T are the density and temperature, respectively. The thermal diffusivity and the kinematic viscosity are computed using a Lewis number of 1.0 and a Prandtl number of 0.7. The gas is assumed to be ideal with a constant specific heat ratio, γ of 1.2196, and a molecular weight, M of 31 kg/kmol. The input parameters from the simplified chemical-diffusive model produce a flame speed, thickness, and temperature of 4.13 m/s, 88.8 μm, and 3487 K, respectively. The resulting detonation velocity (D_{CJ}) is 2200 m/s and the half-reaction thickness is 3.2 μm.

A schematic diagram of the initial conditions is shown in Fig. 1. Initially, a flame (approximated by high-temperature products at 3500K and 1 atm) is placed near the closed end of a rough-walled channel. The channel has a square cross-section with pyramid-shaped roughness elements cut into the walls. The resulting walls in the channel resemble a knurled surface. Quarter-symmetry is assumed and the front and upper surfaces are taken to be symmetry planes. The unobstructed distance between the upper point of the pyramids and symmetry planes is $h = 300$ μm in all cases. Each pyramid has a base, w, of 60 μm and their height, h_p, is varied in a series of simulations from 0 (smooth), 5, 10, 20, 40, and 80 μm to explore the effect of roughness height on DDT. The total height, H, of the domain varies from case-to-case by $H = h + h_p$. No-slip and adiabatic conditions are used on the elements and smooth walls.

The governing equations are solved by a fifth-order accurate Godunov algorithm [14]. An immersed boundary method [15] is used to describe the geometry of the elements. Adaptive mesh refinement [16] is used to refine the grid regions dynamically near shocks, the flame, and the solid surfaces. The simulations described below use 8 computational cells across the y- and z-directions on the coarsest level of refinement and an effective resolution of 64 cells at the finest refinement level. The computational cell size varies slightly from 4.7 to 5.9 μm due to the changing domain height when h_p is varied. The computational mesh is too coarse

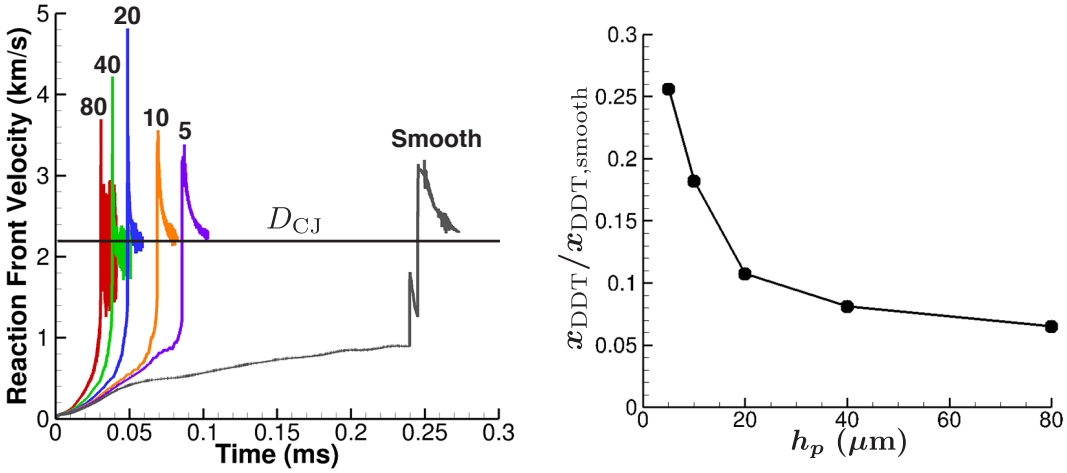

(a) (b)

Figure 2: Computed results showing (a) the elocity of the reaction front as a function of time for different pyramid heights and (b) the normalized DDT run-up distance as a function of roughness element height. The height, h_p of the roughness elements are listed in μm.

to resolve the flow around each of the pyramids for the 5, 10, and 20 μm cases. Nevertheless, these under-resolved pyramids still act as perturbations to the boundary layer, which can influence the acceleration of the flame and transition to detonation. The numerical model was verified and validated against a series of calculations including a variety of Riemann problems and computations of laminar boundary layers, laminar flame propagation, and detonation propagation.

3 Results and Discussion

The velocity of the reaction front as a function of time is shown in Fig. 2(a) for each case. The front velocity relaxes, on average, to the Chapman-Jouget detonation velocity, D_{CJ} after a detonation is formed in each case. Oscillations of the front velocity about D_{CJ} increase with increasing roughness element height. This trend is caused by localized diffraction, failure, and reignition of the detonation as it propagates around each roughness element. The time needed to transition to DDT is significantly reduced by the roughness elements. It takes $\sim$8.3 times longer for the detonation to initiate in the smooth channel than in the rough-walled channel with 80-μm roughness elements.

The run-up distance to detonation, x_{DDT} normalized by the smooth-walled channel run-up distance is shown in Fig. 2(b). The smooth channel case requires 250 full-channel widths ($2h$) for a detonation to initiate. The DDT run-up distance is significantly reduced to 20 and 16 channel-widths for the 40- and 80-μm cases, respectively. The result also indicate that increasing the roughness height beyond 80 μm will likely have a small influence on reducing the DDT run-up distance.

The details of the flame acceleration and detonation initiation mechanisms for the smooth-channel case have been discussed in [5]. Here we focus on the detonation imitation mechanism for the 80-μm case. Isosurfaces of the flame for the $h_p = 80$ μm case are shown in Fig. 3. Planar slices of the temperature field at symmetry plane ($z = H$) and at tips of the roughness elements ($z = h_p$) are shown in Fig. 4.

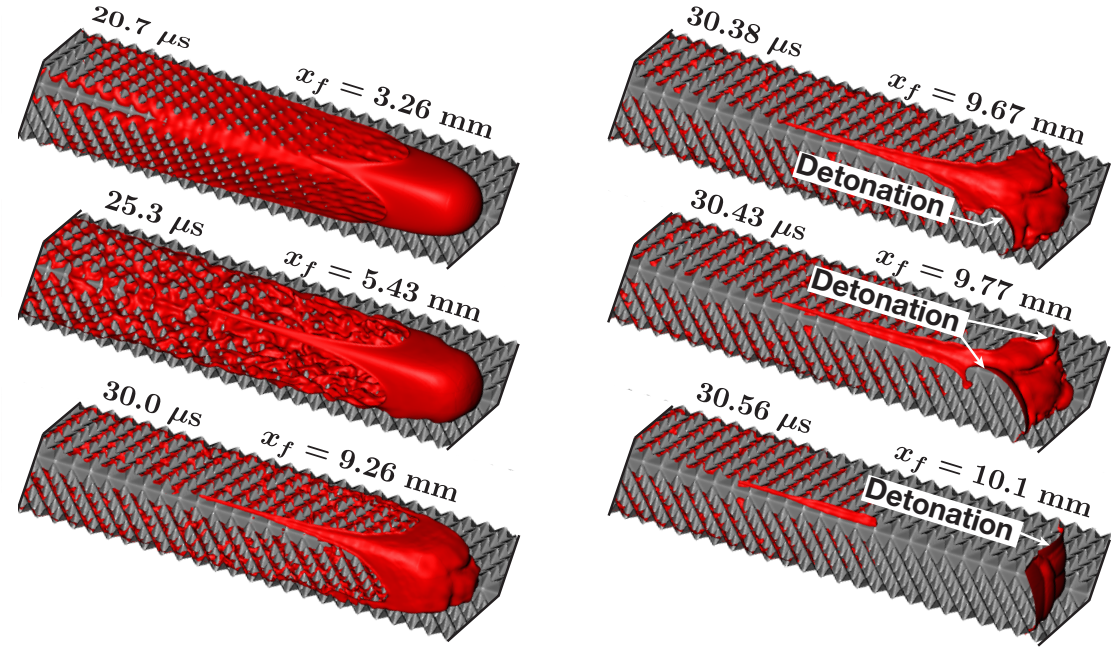

Figure 3: Flame surface, defined by a reactant mass fraction of 0.5, at selected times, in the rough-walled channel with 80 μm-high roughness elements. The time, in μs, and position of the flame tip (x_f), are listed above each instance. Quarter-symmetry is assumed, so only 1/4 of the channel cross section is shown.

The beginning stages of flame acceleration phase and the formation of a tulip flame in the rough-walled channel are similar to those in a smooth-walled channel. One key difference, however, is that the roughness elements can destabilize the boundary layer and promote turbulence. This effect produces the turbulent flame brush near the roughness elements shown in Figure 3 at 25.3 μs.

Figure 4 shows that a precursor shock forms in front of the accelerating flame. A small portion of the precursor shock interacts with the roughness elements and is reflected back towards the flame. Richtmyer-Meshkov and Rayleigh-Taylor instabilities are produced by the interaction between these reflected pressure waves and the flame. (See. Fig. 3 at 30.0 and 30.38 μs.) These instabilities wrinkle the flame and increases the flame area. This, in turn, increases the total fuel consumption rate and provides additional acceleration of the flame.

Intense shear acts on the fluid as it passes between the roughness elements. This viscously heats the gas and raises the temperature in the cavity-like regions between the elements above the shock-heated temperature. Eventually, the combination of shock compression and viscous heating autoignites unburned material in the cavities. Autoignition of the gas in one of these cavities eventually produce effects that lead to detonation. (See Fig. 4 at $z = H$ and 30.2 μs.)

4 Conclusions

Three-dimensional numerical simulations of deflagration-to-detonation in submillimeter channels with adiabatic rough walls were presented. The channels were initially filled with a stoichiometric ethylene and

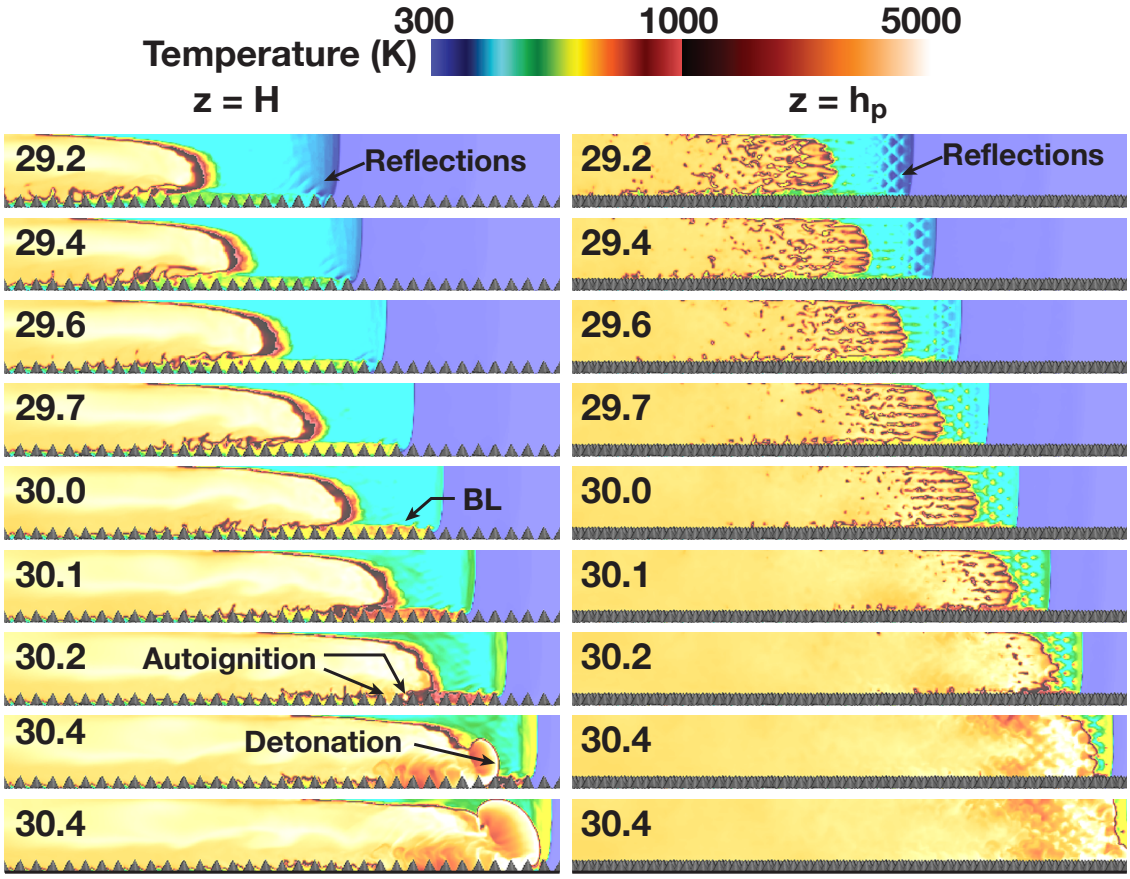

Figure 4: Temperature maps on the symmetry plane ($z = H$) and at the tip of the roughness elements at $z = h_p$. The time, in μs, is shown in the top left of each image.

oxygen mixture at 300 K and 1 atm. The roughness elements were pyramid-shaped, and taken all together, and resemble a knurled surface.

The elements in the rough-walled channels produce shock reflections and intensify turbulence as gas flows around the elements, both of which increase pressure near the flame. In addition, intense shear, produced by gas flowing between the elements, produces a boundary layer-like region and locally heats the unburned material. These conspiring effects lead to a situation where unreacted material autoignites and initiates a detonation. The DDT run-up distance is up to 16 times shorter in the rough-walled channels compared to the smooth-walled channel as a result of turbulence, shock reflections, and enhanced flame acceleration. Examining the influence of channel height and heat loss to the rough walls on DDT is part of our ongoing work.

Acknowledgements

This work was sponsored in part by the Office of Naval Research and the University of Maryland through Minta Martin Endowment Funds in the Department of Aerospace Engineering, and through the Glenn L.

Martin Institute Chaired Professorship at the A. James Clark School of Engineering. The authors acknowledge the University of Maryland supercomputing resources (http://www.it.umd.edu/hpcc) made available in conducting the research reported in this paper. The authors particularly acknowledge the help of Mr. Alp Ozgen in determining the optimal chemical-diffusive model for ethylene and oxygen.

References

[1] G. Ciccarelli, S. Dorofeev, Prog Energ Combust 34 (4) (2008) 499 – 550.

[2] P. Wolański, P Combust Inst, 34 (1) (2013) 124–158.

[3] M.-H. Wu, T.-H. Lu, J Micromech Microeng 22 (10) (2012) 105040.

[4] Z.-E. Chen, M.-H. Wu, Proceedings of 24$^{\text{th}}$ ICDERS, Paper 114, Taipei, Taiwan, 2013.

[5] R. W. Houim, A. Ozgen, and E. S. Oran, "The role of spontaneous waves in the deflagration-to-detonation transition in submillimetre channels," *Combust Theor Modelling* (2016)

[6] M. Ivanov, A. Kiverin, I. Yakovenko, M. Liberman, Int J Hydrogen Energ 38 (36) (2013) 16427–16440.

[7] L. Kagan, P. Gordon, G. Sivashinsky, P Combust Inst 35 (1) (2015) 913 – 920.

[8] M. Liberman, M. Ivanov, A. Kiverin, M. Kuznetsov, A. Chukalovsky, T. Rakhimova, Acta Astronaut 67 (7–8) (2010) 688 – 701.

[9] M. H. Wu, M. Burke, S. Son, R. Yetter, Proc Combust Inst 31 (2) (2007) 2429 – 2436.

[10] M.-H. Wu, W.-C. Kuo, P Combust Inst 34 (2) (2013) 2017 – 2024.

[11] E. Oran, V. Gamezo, Proceedings of 21$^{\text{th}}$ ICDERS, Montreal, Canada, 2005.

[12] E. Dziemińska, A. K. Hayashi, J Hydrogen Energ 38 (10) (2013) 4185 – 4193.

[13] K. Shchelkin, J Exp Theor Phys 10 (1940) 823–827.

[14] R. W. Houim, K. K. Kuo, J Comput Phys 230 (23) (2011) 8527–8553.

[15] A. Chaudhuri, A. Hadjadj, A. Chinnayya, J Comput Phys 230 (5) (2011) 1731 – 1748.

[16] Center for Computational Sciences and Engineering, University of California, Berkeley, available at <https://ccse.lbl.gov/index.html> (Retrieved 03-2015).